Supplementary methods

B. J. Davies[1]**, J. L. Carrivick**[2]**, N. F. Glasser**[1]**, M. J. Hambrey**[1]**, and J. L. Smellie**[3]

[1]Centre for Glaciology, Institute for Geography and Earth Sciences, Aberystwyth University, Llandinam Building, Penglais Campus, Aberystwyth SY23 3DB
[2]Department of Geography, University of Leeds, Leeds LS2 9JT
[3]Department of Geology, University of Leicester, Leicester LE1 7RH

Correspondence to: B. J. Davies
(bdd@aber.ac.uk)

1 Introduction

In order to accurately map individual glacier drainage basin polygons, ice divides were mapped through analysis of glaciological mapping and the SPIRIT DEMs (identifying cols, high points and breaks in slope; using models of aspect and slope; and using hydrological tools in Arc-
5 Toolbox (Basin, Fill, Flow Direction, Watershed) to automatically determine surface flow and drainage basins). Glacier drainage basin mapping followed four stages. First, glaciers less than 0.1 km^2 were excluded from this study because of difficulties in identification, accurate mapping, and the danger of misclassification of snow patches. The availability of multi-temporal images (Table S1) aided the identification of perennial snow (noted in *Remarks* in the GLIMS
10 geodatabase; www.glims.org), which shows no bare ice at any point (cf. Paul et al., 2010). Initial structural glaciological mapping aided the identification of ice divides and flow unit boundaries. Glaciological structures were identified on the 2009 ASTER and 2006 SPOT-5 images (Fig. S1; Table S1) according to previously published criteria (Glasser et al., 2009, 2011). Finally, analysis of the SPIRIT DEM (models of aspect, slope and drainage; Fig. S1; cf. Svoboda and Paul,
15 2009; Bolch et al., 2010) aided the identification of the drainage basins, which were digitised as separate polygons.

Attribute data was generated for each glacier. Polygon surface area (km^2) was automatically derived in the GIS. Glacier *Length* was measured along the centre-line profile. In the accumulation area, *Length* follows the steepest downward gradient. Where identifiable, glacier length
20 was also measured along surface-flow trajectories. The same route was followed for each year the glacier length was measured. Glacial length mapping is accurate to 3 pixels, i.e., 45 m for ASTER images (Table S2), and an error margin of $\pm$ 22.5 m was therefore applied to either side of the digitised line. In glaciers with multiple cirques and accumulation areas, Length was measured according to the longest distance. Ice caps and ice fields were not measured.
25 *Primary Classification* and *Remarks* are glacier morphology descriptors with a specific number of classes, and conform to published criteria (Rau et al., 2005). Primary classes include continental ice sheet, ice field, ice cap, outlet glacier, valley glacier, mountain glacier, glacieret or snowfield, ice shelf, rock glacier (not included in this analysis) or ice stream. Form com-

prises the descriptors, compound basin(s), simple basin, cirque, niche, crater, ice apron, group or remnant (Rau et al., 2005). The *Remarks* attribute column is a four-digit code representing a brief glacier description, representing snow cover, calving margin characteristics, surging behaviour and ice divide characteristics (refer to Paul et al., 2010). Frontal characteristics includes information on the terminus (lobed, calving, land-terminating, coalescing; cf. Rau et al., 2005).

Median Elevation is equal to the area-weighted mean value, and is the elevation that divides the glacier into two equal parts (H_{MEDIAN}). This is calculated in the GIS by counting the 'Elevation' values of all pixels that fall within the glacier boundaries. Mean Elevation (H_{MEAN}) is equal the summation of all elevation values in the DEM and the division by the number of cells. However, the World Glacier Inventory (WGI) contains the arithmetic mean ($MEAN_{ECR}$), which is the midpoint elevation between maximum and minimum elevations. Paul and Svoboda 2009 found that the automatic derivation of mean altitude from the DEM was closely correlated to the arithmetic mean, and in this dataset, the correlation was very strong ($r^2 = 0.8$; p value less than 0.001; Table 5). H_{MEAN} was therefore used as a proxy for mean elevation throughout this paper.

Models of aspect and slope were derived from manipulation of the 2006 SPIRIT DEMs. Zonal functions in ArcGIS were then used to compute the Mean Slope for each glacier polygon. Mean Slope as derived from DEM zonal statistics has been shown to correlate very well with other methods of calculating mean slope (for example, length and elevation range) (Paul and Svoboda, 2009), and can be a good proxy for mean thickness (Paul et al., 2010).

The aspect, or orientation, of a glacier is useful for modelling, particularly when used in conjunction with glacier altitude (Evans, 2006), and is a standard parameter in glacier inventories (Schiefer et al., 2008; Svoboda and Paul, 2009; Bolch et al., 2010). Automatic derivation of slope and aspect from zonal statistics on a DEM allows greater impartiality and objectivity, and is recommended for glacier inventories (Manley, 2008; Racoviteanu et al., 2009; Paul and Svoboda, 2009). However, as aspect is a circular parameter, mean values must be derived through decomposition with the sine and cosine values (Paul et al., 2010). The original method used is detailed in Table S2.

Glacier hypsometric curves were calculated by masking glacier polygons with the 40 x 40

3

m resolution SPIRIT DEM. Raster DEMs for each glacier polygon of interest were generated. Hypsometry was calculated by summing pixels within 100 m elevation interval bins (as recommended by Paul et al., 2010), using the histogram function in Spatial Analyst in ArcMap 9.3, and by multiplying the resulting number of pixels in each elevation bin by pixel area ($1600\,\mathrm{m}^2$).

5 Hypsometric curves of cumulative area (km^2) for each 100 m elevation interval could then be plotted. As this is very time consuming, this parameter was only applied to glaciers over 40 km^2. Normalised hypsometric curves were therefore created for 54 of the 194 glaciers.

2 Equilibrium line altitude estimation

Five methods of long-term ELA estimation were explored (Table 3). As the Median Elevation
10 (H_{MEDIAN}) divides the glacier into two equal parts, it represents an accumulation-area ratio (AAR) of 50%, and has frequently been used as a proxy for ELA in simple valley glaciers. Median altitude correlates well with the balanced-budget ELA (Braithwaite and Raper, 2009; Paul and Svoboda, 2009). However, it does not take into account variations in the area/altitude distribution (i.e. glacier hypsometry). This method ($\mathrm{ELA_{MEDIAN}}$) was applied to all glaciers.

15 The long-term ELA can also be calculated by assuming an AAR of 0.6 ($\mathrm{ELA_{AAR}}$), as 0.6 is assumed to indicate steady-state conditions (Torsnes et al., 1993). As this method is labour-intensive, it was only applied to the 54 glaciers that exceed 40 km^2. It is important to note that the AAR may be ineffective for calculating the ELA for marine-terminating glaciers (Leonard and Fountain, 2003). This method used the previously-created hypsometric curves for each in-
20 dividual glacier. The 100 m contour that was below 60% of the cumulative area was calculated.

Toe to Headwall Ratio ($\mathrm{ELA_{THAR}}$) has been used for ELA calculations on small Alpine (Carrivick and Brewer, 2004) and Norwegian glaciers, and uses the ratio between the minimum and maximum altitude of the glacier. A constant of 0.4 has previously been used (Dahl and Nesje, 1992; Torsnes et al., 1993). This method works best on small cirque glaciers.

25 The 'Hess' method (Hess, 1904) (also known as the 'geodetic' method; Jiskoot et al., 2009) is determined from the transition of convex to concave contours. In alpine land-terminating glaciers, the accumulation zone of a glacier is bowl-shaped (convex-down), as snow and ice

advects inwards (Leonard and Fountain, 2003). In the ablation zone, the contours are convex, as mass is lost from the sides. The flat transitional area is equivalent to the long-term average ELA. This method has been applied successfully to a number of glacier inventories (Leonard and Fountain, 2003; Jiskoot et al., 2009). In this study, 20 m contours were derived from the 2006 SPIRIT DEM. The first up-glacier concave contour, counted from the glacier toe, was taken as a proxy for the long-term ELA. We used a point shapefile with a point located where this contour crosses the centre maximum flowline (i.e. *Length*) to create a dataset for ELA_{HESS}. In some cases, there was no discernible difference between the shape of the contours down glacier; these glaciers were omitted from the analysis. The method was difficult to apply in the case of glaciers with complex or compound cirques, may not be applicable to marine-terminating glaciers, and it cannot be applied to those glaciers with steep ice falls or ending in steep ice cliffs (Jiskoot et al., 2009), thereby limiting the applicability of the Hess method. The shape of the glaciers on James Ross Island is strongly controlled by the bedrock geology, with very steep bedrock cliffs forming icefalls at the head of the cirques, therefore excluding the 'Hess' method. The ELA_{HESS} method was therefore only applied to 69 out of 194 glaciers, although it may only be applicable to 13 land-terminating Alpine-style glaciers.

The snow line at the end of the melt season fluctuates annually, but mapping of the snow line (firn line) at the end of the ablation season may be a proxy for ELA in that year (Rivera et al., 2007; Jiskoot et al., 2009). In Alpine glaciers, this 'firn line' is closely related to the ELA, if the ELA has maintained a constant position for several years (Braithwaite and Raper, 2009). By mapping the end-of-season snow line over several years and by using the minimum value, the Transient Snow Line (TSL) may be a proxy for the long-term average ELA (ELA_{TSL}). However, snow lines vary enormously not only annually but also monthly and daily; this can lead to large errors if the TSL is mapped directly before or after a snowfall event, which occurs throughout the polar summer season. Snow may be difficult to differentiate from superimposed ice on satellite images in polar regions without SAR imagery (although it is simply identified in the field, as superimposed ice lacks foliation) (König et al., 2002; Benn and Evans, 2010). In addition, cloud-free scenes are not available for all glaciers for all years in the study region.

ASTER and SPOT-5 scenes with maximum coverage, and minimal snow and cloud cover

5

were chosen to map snowlines. The only suitable images were from 2006 (January, February, December) and January 2002 (cf. Table S1). Snow lines were manually digitised as polylines with a 15 m buffer (cf. Jiskoot et al., 2009), providing the minimum, maximum, mean and standard deviation elevation of the snow line for each glacier for each of the years mea-
5 sured (elevation values were determined from the 2006 SPIRIT DEM). The minimum snowline elevation for each year surveyed was then used to calculate mean ELA_{TSL}. The standard deviations provided error estimations and an indication of accuracy. The mean of the ELA from mapped snowlines from several years (ELA_{TSL}) was calculated. This method was applied to 144 glaciers.

10   Finally, ELAs are ideally measured on glaciers that are in a balanced state (Osmaston, 2005). Our study has shown that almost all the glaciers analysed are retreating and are therefore in a state of negative mass balance. In addition, estimating the ELA of polar tidewater glaciers is difficult, because these glaciers terminate in the ocean, and their mass flux is controlled by calving processes, instead of direct climatological factors. It is clear that remote methods
15 of ELA determination require further testing against real mass-balance data in this region to validate their reliability.

3   Calculation of glacier change

Glacier area and length was mapped for 1988, 1997, 2001, and 2009, using ASTER and LAND-SAT images (Table S1) and the Antarctic Digital Database (ADD). Where the snow or cloud
20 cover made mapping impossible, a LANDSAT image from 1990 or ASTER images for 2002 were used. The date of the satellite imate used to map each glacier is included in the database (from www.glims.org). A buffer width of 3 pixels was applied around the outline for each glacier, providing an error margin for each result (Table 2). However, as we assume no migration of ice divides, this produces an unnecessarily large absolute error for each subsequent year
25 of analysis. We therefore also used a 3-pixel wide buffer only around the frontal margin of the glacier in order to capture errors in mapping the change in glacier snout position. Both error margins are included in the database.

Following GLIMS guidelines (Racoviteanu et al., 2009; Raup and Khalsa, 2010), PGIS was defined as an 'ice tongue', with significant ice input from the land surface. This floating ice mass extends from and coalesces with ice from several tidewater glaciers (e.g. Sjögren Glacier and Röhss Glacier). It was therefore divided up and considered part of the various tributary glaciers. Ice divides on PGIS are identified through structural glaciological mapping.

References

Benn, D.I., and Evans, D.J.A., 2010. Glaciers & Glaciation. London, Hodder Education, 802 pp.

Bolch, T., Menounos, B., and Wheate, R.: Landsat-based inventory of glaciers in western Canada, 1985-2005. Remote Sensing of Environment 114, 127-137, 2010.

Braithwaite, R.J. and Raper, S.C.B.: Estimating equilibrium-line altitude (ELA) from glacier inventory data. Annals of Glaciology 50, 127-132, 2009.

Carrivick, J.L. and Brewer, T.R.: Improving local estimations and regional trends of glacier equilibrium line altitudes. Geografiska Annaler 86 A, 67-79, 2004.

Dahl, S.O., and Nesje, A.: Paleoclimatic implications based on equilibrium-line altitude depressions of reconstructed Younger Dryas and Holocene cirque glaciers in inner Nordfjord, western Norway. Palaeogeography, Palaeoclimatology, Palaeoecology 94, 87-97, 1992.

Evans, I.S.: Local aspect asymmetry of mountain glaciation: A global survey of consistency of favoured directions for glacier numbers and altitudes. Geomorphology 73, 166-184, 2006.

Glasser, N.F., Kulessa, B., Luckman, A., Jansen, D., King, E.C., Sammonds, P.R., Scambos, T.A., and Jezek, K.C.: Surface structure and stability of the Larsen C Ice Shelf, Antarctic Peninsula. Journal of Glaciology 55, 400-410, 2009.

Glasser, N.F., Scambos, T.A., Bohlander, J.A., Truffer, M., Pettit, E.C., and Davies, B.J.: From ice-shelf tributary to tidewater glacier: continued rapid glacier recession, acceleration and thinning of Röhss Glacier following the 1995 collapse of the Prince Gustav Ice Shelf on the Antarctic Peninsula. Journal of Glaciology 57, 397-406, 2011.

Hess, H.: Die Gletscher. Braunschweig, Vieweg & Sohn, 220 pp, 1904

Jiskoot, H., Curran, C.J., Tessler, D.L., and Shenton, L.R.: Changes in Clemenceau Icefield and Chaba Group glaciers, Canada, related to hypsometry, tributary detachment, length-slope and area-aspect relations. Annals of Glaciology 50, 133-143, 2009.

König, M., Wadham, J., Winther, J.-G., Kohler, J., and Nuttall, A.-M.: Detection of superimposed ice

on the glaciers Kongsvegen and midre Lovnbreen, Svalbard, using SAR satellite imagery. Annals of Glaciology 34, 335-342, 2002.

Leonard, K.C., Fountain, A.G.: Map-based methods for estimating glacier equilibrium-line altitudes. Journal of Glaciology 49, 329-336, 2003.

5 Manley, W.F.: Geospatial inventory and analysis of glaciers: a cast study for the eastern Alaska Range. US Geological Survey Professional Papers 1386-K, K424-K429, 2008.

Osmaston, H.: Estimates of glacier equilibrium line altitudes by the Area x Altitude, the Area x Altitude Balance Ratio and the Area x Altitude Balance Index methods and their validation. Quaternry International 138-139, 22-31, 2005.

10 Paul, F. and Svoboda, F.: A new glacier inventory on southern Baffin Island, Canada, from ASTER data: II. Data analysis, glacier change and applications. Annals of Glaciology 50, 22-31, 2009.

Paul, F., Barry, R.G., Cogley, J.G., Frey, H., Haeberli, W., Ohmura, A., Ommanney, C.S.L., Raup, B., Rivera, A., and Zemp, M.: Guidelines for the compliation of glacier inventory data from digital sources, GLIMS, Global Land Ice Measurement from Space, NSIDC, 23 pp., 2010.

15 Racoviteanu, A.E., Paul, F., Raup, B., Khalsa, S.J.S., and Armstrong, R.: Challenges and recommendations in mapping of glacier parameters from space: results of the 2008 Global Land Ice Measurements from Space (GLIMS) workshop, Boulder, Colorado, USA. Annals of Glaciology 50, 53-69, 2009.

Rau, F., Mauz, F., Vogt, S., Khalsa, S.J.S., and Raup, B.: Illustrated GLIMS Glacier Classification Manual, Version 1.0. GLIMS Regional Centre, 'Antarctic Peninsula', GLIMS (Global Land Ice Measurement from Space), NSIDC, 36 pp., 2005.
20

Raup, B., and Khalsa, S.J.S.: GLIMS Analysis Tutorial. www.GLIMS.org, GLIMS, Global Land Ice Measurements from Space, NSIDC, 15 pp., 2010.

Rivera, A., Benham, T., Casassa, G., Bamber, J., Dowdeswell, J.A.: Ice elevation and areal changes of glaciers from the Northern Patagonia Icefield, Chile. Global and Planetary Change 59, 126-137, 2007.

25 Schiefer, E., Menounos, B., and Wheate, R.: An inventory and morphometric analysis of British Columbia glaciers, Canada. Journal of Glaciology 54, 551-560, 2008.

Svoboda, F. and Paul, F.: A new glacier inventory on southern Baffin Island, Canada, from ASTER data: I. Applied methods, challenges and solutions. Annals of Glaciology 50, 11-21, 2009.

Torsnes, I., Rye, N., Nesje, A.: Modern and Little Ice Age Equilibrium-Line Altitudes on outlet valley
30 glaciers from Jostedalsbreen, Western Norway: an evaluation of different approaches to their calculation. Arctic and Alpine Research 25, 106-116, 1993.
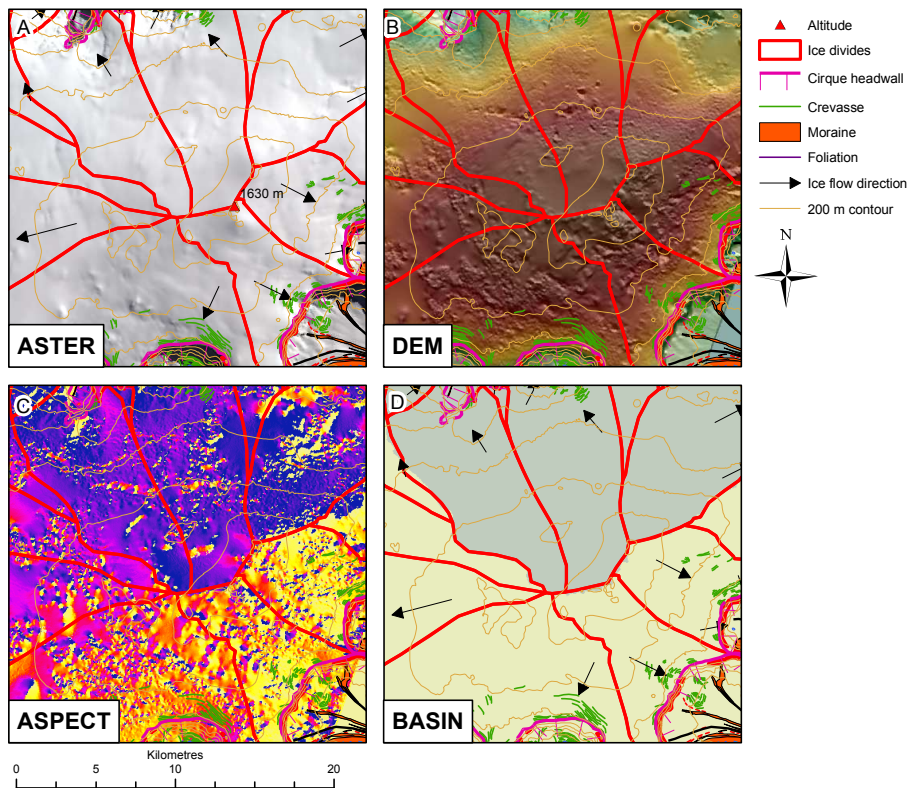
Fig. S1. Delineation of ice divides on the centre of James Ross Island, Mount Haddington Ice Cap. Delineation of ice divides used a combination of structural glaciological mapping from ASTER and SPOT-5 images (A), analysis of ASTER images and (B) the 2006 SPIRIT DEM showing high and low points and topographic divides, models of aspect (C) and slope, and (D) automatic drainage basin delineation using hydrological tools.

Table S1. SPOT-5 and ASTER scenes used in the analysis of glacier change and estimates of cloud cover (visually estimated). TP = Trinity Peninsula. JRI = James Ross Island. VI = Vega Island.

Sensor	Date	Region	Scene ID	Path/Row	Cloud cover
SPOT-5	23/01/2006	JRI	GES 08-025 James Ross Island		5%
SPOT-5	07/0/2006	TP	SPI-09-049 Antarctic Peninsula		5%
ASTER	06/02/2009	Sjögren Glacier	AST_L1A0032070439415, AST_L1B00302062009130938	216/105	10-20%
ASTER	03/03/2009	JRI	AST_L1A0032071357944, AST_L1B00303032009130328	216/105	0%
ASTER	03/03/2009	Joinville Island	AST_L1A0032071358554, AST_L1B00303032009130319	216/104	30%
ASTER	13/12/2008	Joinville Island	AST_L1A0032068532209, AST_L1B00312132008130309	216/104	0%
ASTER	23/03/2008	JRI and eastern TP	AST_L1A0032072667022, AST_L1B00303232008130815	216/105	10%
ASTER	29/12/2002	JRI	AST_L1A0032010352317, AST_L1B00312292002130340	216/105	50%
ASTER	29/12/2002	Joinville Island	AST_L1A0032010352317, AST_L1B00312292002130340	216/104	40%
ASTER	05/03/2002	Northern TP	AST_L1A0032006163082, AST_L1B00303052002132218	216/105	20% in NE corner
ASTER	18/01/2002	JRI and eastern TP	AST_L1A0032005839335, AST_L1B00301182002131108	216/105	30% over western TP
ASTER	08/01/2001	JRI	AST_L1A0032004102903, AST_L1B00301082001131449	216/105	0%
ASTER	14/02/2001	TP	AST_L1A0032005033375, AST_L1B0030214200113238	216/105	20% over the sea
ASTER	15/11/2001	Southern TP	AST_L1A0032005556226, AST_L1B00311152001131252	216/105	Up to 50%
ASTER	26/09/2001	Western TP	AST_L1A0032004337049, AST_L1B00309262001132645	216/105	10%

Table S2. Method for calculation of mean glacier aspect from a DEM using automatic methods in ArcGIS

Step	Tool	Method and notes
1.	3D Analyst → Surface analysis → Aspect	Create a new model of aspect from the DEM ("apis_aspect")
2.	Data Management Tools → Raster → Raster Dataset → Create Raster Dataset	Create a new blank raster (e.g. "apis_blank")
3.	3D Analyst → Reclassify	Reclassify each pixel value to 1 and save, e.g., "apis_reclass"
4.	Spatial Analyst → Raster Calculator	Apis_reclass = sin([apis_aspect] div deg). Export to geodatabase ("sine_aspect")
6.	Repeat for cosine	Create cosine model with mean values for each glacier. Join the tables.
7.	Add field ("sine_div_c") → Field Calculator	Calculate mean_sine / mean_cos
8.	Add Field ("angle") (set as double) → Field Calculator → "Advanced"	*Pre-VBA Script Code:* Dim arctan as double. Arctan = Atn ([sine_div_c]). angle = arctan * 180 / 3.141592654. *Value Output:* angle
9.	Add Field (aspect_ang). Set as double. Field Calculator → "Advanced"	*Pre-Logic VBA Script Code:* If [mean_sine] > 0 And [mean_cos] > 0 Then angle = [angle]. ElseIf [mean_cos] < 0 Then angle = [angle] + 180. ElseIf [mean_sine] < 0 And [mean_cos] > 0 Then angle = [angle] + 360. Else angle = -1. EndIf. *Value Output:* angle
11.	Join table to glacier polygons	No fields should have a value of -1 (which is used as a check). Check by displaying angles as orientated arrows (Display - Quantities - Graduated Symbols).

11